

Published in final edited form as:

*Oral Oncol.* 2013 June ; 49(6): 582–590. doi:10.1016/j.oraloncology.2013.01.009.

## Ex vivo Confocal Imaging with Contrast Agents for the Detection of Oral Potentially Malignant Lesions

S. El Hallani<sup>1</sup>, C. F. Poh<sup>1,2</sup>, C. E. Macaulay<sup>1</sup>, M. Follen<sup>3</sup>, M. Guillaud<sup>1</sup>, and P. Lane<sup>1</sup>

<sup>1</sup>British Columbia Cancer Research Centre, Integrative Oncology department and Cancer Imaging unit, Vancouver, BC, V5Z 1L3 Canada

<sup>2</sup>Faculty of Dentistry, University of British Columbia, Vancouver, BC, V6T 1Z3 Canada

<sup>3</sup>Department of Obstetrics and Gynecology, Texas Tech University Health Sciences Center, Paul L. Foster School of Medicine, El Paso, TX 79905, USA

### Abstract

**Objectives**—We investigated the potential use of real-time confocal microscopy in the non-invasive detection of occult oral potentially malignant lesions. Our objectives were to select the best fluorescence contrast agent for cellular morphology enhancement, to build an atlas of confocal microscopic images of normal human oral mucosa, and to determine the accuracy of confocal microscopy to recognise oral high-grade dysplasia lesions on live human tissue.

**Materials and Methods**—Five clinically used fluorescent contrast agents were tested in vitro on cultured human cells and validated ex vivo on human oral mucosa. Images acquired ex vivo from normal and diseased human oral biopsies with bench-top fluorescent confocal microscope were compared to conventional histology. Image analyzer software was used as an adjunct tool to objectively compare high-grade dysplasia versus low-grade dysplasia and normal epithelium.

**Results**—Acriflavine Hydrochloride provided the best cellular contrast by preferentially staining the nuclei of the epithelium. Using topical application of Acriflavine Hydrochloride followed by confocal microscopy, we could define morphological characteristics of each cellular layer of the normal human oral mucosa, building an atlas of histology-like images. Applying this technique to diseased oral tissue specimen, we were also able to accurately diagnose the presence of high-grade dysplasia through the increased cellularity and changes in nuclear morphological features. Objective measurement of cellular density by quantitative image analysis was a strong discriminant to differentiate between high-grade dysplasia and low-grade dysplasia lesions.

**Conclusions**—Pending clinical investigation, real-time confocal microscopy may become a useful adjunct to detect precancerous lesions that are at high risk of cancer progression, direct biopsy and delineate excision margins.

---

© 2013 Elsevier Ltd. All rights reserved.

Correspondence: Dr. Soufiane El Hallani, Address: Department of Pathology and Laboratory Medicine, 501 Smyth Road, The Ottawa Hospital-General Campus, Ottawa, ON, K1H 8L6 Canada, Phone: (001) 613-316-9238, Fax: (001) 613-562-5422, soufiane.elhallani@yahoo.ca.

#### Conflict of interest statement

None declared.

**Publisher's Disclaimer:** This is a PDF file of an unedited manuscript that has been accepted for publication. As a service to our customers we are providing this early version of the manuscript. The manuscript will undergo copyediting, typesetting, and review of the resulting proof before it is published in its final citable form. Please note that during the production process errors may be discovered which could affect the content, and all legal disclaimers that apply to the journal pertain.

## Keywords

Confocal microscopy; contrast agent; oral dysplasia

---

## INTRODUCTION

There is a growing recognition of the need to develop new strategies for oral cancer control. Each year more than 300,000 new cases of oral cancer are identified worldwide<sup>1</sup>, and over 40,000 of these cases are from the United States<sup>2</sup>. The recurrence and formation of second cancers are frequent (10–25% of cases)<sup>3</sup>. Even when successful, the treatment of late-stage oral cancer can be devastating to the patient's quality of life. It is critical that we begin to detect this disease at its earliest possible state and to manage it more effectively.

Oral potentially malignant lesions (mild dysplasia; moderate dysplasia; severe dysplasia or carcinoma *in situ*) present clinically as a heterogeneous group of lesions, most often forming either white (leukoplakia) or red patches (erythroplakia)<sup>4</sup>. At present, the initial decision that a change in the oral mucosa requires further assessment is still made on the basis of clinical appearance. The actual assignment of risk requires a biopsy and a determination of the presence and degree of dysplasia. The potentially malignant lesions are classified as high-grade dysplasia (severe dysplasia) and low-grade dysplasia (combining mild and moderate dysplasia). Many low-grade dysplasia, especially mild dysplasia, do not progress to cancer; high-grade dysplasia; however, often progresses to invasive squamous cell carcinoma if left untreated and necessitates early detection and management. It can be challenging for the clinician to differentiate abnormalities or at-risk lesions that require a biopsy from reactive lesions (infection and inflammation). If the lesion is extensive it may be prudent to biopsy more than one area to ensure that the highest degree of histology can be made. A non-representative biopsy would delay the chance of early detection and treatment. Moreover, the molecular risk stratification of low-grade dysplasia in reference to the loss of heterozygosity<sup>5</sup> and the quantitative pathology have shed light on how to predict the clinical differences in histologically similar lesions<sup>6</sup>. The decision on where to biopsy is increasingly critical. Ideally, biopsies should be limited to both targeted samplings of relevant lesions and areas with the highest grade and/or risk. Therefore, there is an urgent need for the development of new technologies that can help the clinician identify the most accurate site of precancerous lesions, especially those in high-grade areas, which are the most susceptible to progress into invasive squamous cell carcinoma<sup>7</sup>.

Laser scanning confocal microscopy is an emerging imaging technology to enable the detection of intraepithelial neoplasia<sup>8–10</sup>. This optical technique has sufficient resolution and contrast to produce images of individual cells and nuclei in thick sections of tissue after the application of fluorescent contrast agents<sup>11</sup>. Optical sections similar to the histological analysis of biopsy specimens are imaged on a focal plane and at various depths below the surface without tissue removal. Moreover, digital images can be acquired in real time, enhancing its potential use in the clinic for directing biopsy acquisitions, delineating excision margins and surveillance.

This study describes the pre-clinical use and evaluation of confocal microscopy in the non-invasive detection of oral dysplasia. The work aimed (i) to assess the ability of commonly used contrast agents to enhance cellular morphology and tissue architecture of the oral epithelium, (ii) to appreciate a normal histology of human oral mucosa using confocal imaging, (iii) to examine the accuracy of the technique to recognise high-grade dysplasia through its correlation with conventional histology, and (iv) to evaluate the contribution of

image analyzer on acquired confocal images to objectively discriminate between high-grade and low-grade dysplasia.

## MATERIALS AND METHODS

### Cell Culture

Four types of human cells were used in this study: normal bronchial epithelial cells from primary culture (NHBE), in vitro spontaneously-transformed keratinocytes from normal skin (HaCaT), and cancer cell lines from squamous cell carcinoma of the tongue (SCC-15) and of the cervix (HeLa). NHBE cells were purchased from Lonza (Walkersville, MD) and cultured through one passage in SingleQuots supplemented Bronchial Epithelial Growth Media (Lonza, Walkersville, MD). HaCaT is a gift from Dr. CF.P. HeLa and SCC-15 cells were obtained from the American Type Culture Collection (Rockville, MD). HaCaT and HeLa cells were cultured in Dulbecco's modified eagle media (DMEM) growth medium with supplements of 10% fetal bovine serum and 1% Penicillin/Streptomycin (GIBCO, Grand Island, NY). SCC-15 cells were cultured in DMEM and Ham's F12 (GIBCO, Grand Island, NY) with 10% fetal bovine serum and 1% Penicillin/Streptomycin. Once the cells were 75–80% confluent, they were dissociated with 0.25% trypsin (GIBCO, ON) and seeded onto sterile glass slides covered by the growth medium. After 24 hours of incubation, the slides were gently washed with phosphate-buffered saline (PBS), prior to staining and confocal imaging.

### GFP-H2B transfected HeLa cells

HeLa cells were grown as monolayers in 10 cm Petri dishes. Exponentially growing cells were transfected with 20ug H2B–GFP expression vector (Addgene, MA) using a calcium phosphate precipitation protocol<sup>12</sup>. Transfected cells were re-plated 48 hours after transfection and 0.5mg/ml Geneticin (GIBCO, ON) was added 72 hours after transfection to select colonies of resistant cells. The selective medium was changed every 2 – 4 days. After 15 days of drug selection, surviving colonies were checked under fluorescence microscopy, and the GFP-positive colonies were isolated.

### Human oral mucosa ex vivo specimens

Oral specimens (n=31) were obtained from participants in the Terry Fox Research Institute-funded COOLS trial (TFRI2009-24)<sup>13</sup>. Informed consent was obtained from all participants. The protocol was approved by the Review of Ethics Board of the British Columbia Cancer Agency and the University of British Columbia (H11-00011). Immediately following oral surgery intraoperatively, 5 × 5 mm paired samples from the lesion and margin were obtained and placed in a Petri dish on a small piece of 10% PBS-moistened gauze and then transported to the imaging laboratory.

The mucosal surface of the specimens was topically stained with contrast agents of 1% Cresyl Violet acetate (CV, Sigma-Aldrich) and 0.05% Acriflavine Hydrochloride (AH, Fluka), as per the staining and imaging protocol discussed in the next section. The specimen was placed on a glass slide with the epithelial surface (superficial layer of the oral mucosa) facing the objective lens of a confocal microscope and *en face* images were acquired. A cover glass was placed on the specimens to prevent the tissue from adhering to the objective lens. Imaging was completed within 2 hours of tissue removal. After imaging, all the specimens were formalin-fixed and paraffin-embedded. Hematoxylin and Eosin (H&E) stained tissue sections were prepared for histopathological assessment by an experienced oral pathologist (CFP). H&E slides were photographed on a Nikon Eclipse microscope. Color images were recorded and processed using a CCD camera (MicroPublisher 3.3, Q-Imaging).

## Staining and imaging protocol

Five fluorescent stain solutions were prepared by dissolving powder dyes in 10% PBS at specific concentrations (w/v): 1% Cresyl Violet acetate (CV, Sigma-Aldrich), 1% Methylene Blue (MB, Fischer Scientific), 1% Toluidine Blue (TB, Fisher Scientific), 0.05% Acriflavine Hydrochloride (AH, Fluka), and 0.2% Fluorescein Sodium (FS, Fluka). The solutions were filtered using a 0.2  $\mu\text{m}$  pore-sized sterilization filter to remove any undissolved compounds. These stains were tested in cultured cells and human oral ex vivo specimens (only CV and AH) by topical application onto the slides or the epithelium surface of oral specimens. The incubation time was 2 minutes. Then the samples were washed with PBS for 5 minutes.

Confocal fluorescence microscopy was performed on a bench-top Carl Zeiss Axio Imager Z1 equipped with a custom laser-scanning confocal attachment. The custom confocal attachment employed a resonance scanner and galvanometer (Cambridge Technology) for laser scanning, an Avalanche photodiode (Hamamatsu) for detection, and a frame grabber (Matrox) to digitize the signal. A laser excitation light was provided by a 488nm laser (Coherent), 561nm laser (Melles Griot) and 638nm (red) laser (Melles Griot). All the images were acquired using a 25X/0.80 water-immersion objective lens. The time interval between the topical application of the stain and the completion of the confocal imaging was typically about 10 minutes.

## Image analysis for quantitative pathology

Gray-scale confocal images (N=94, 41 normal, 11 hyperplasia, 15 mild dysplasia, 9 moderate dysplasia, 18 severe dysplasia) were analyzed by Getafics image analyzer software. The Getafics system was developed *in-house* as previously described<sup>14</sup>. Briefly, TIFF confocal images were uploaded in the software platform. Automatic or semi-automatic segmentation algorithms were used to detect the center of gravity of the nuclei which were then used as points to generate the Voronoi diagram, a geometric model of the tissue from which numerous architectural features can be extracted from and exported for to excel file for further statistical analysis usage. In this study, we are interested to use this technique to objectively quantify the cell density. All statistical significance was assessed using ANOVA and performed using STATISTICA software (StatSoft Inc., Tulsa, OK).

## RESULTS

### Contrast agents enhance the observation of nuclear distribution and features using confocal microscope

We used a simple in vitro system for the evaluation of the contrast agents. Acriflavine Hydrochloride (AH) and Fluorescein Sodium (FS) fluoresced at 488nm excitation wavelength, Cresyl Violet (CV) fluoresced at 561nm excitation wavelength, and Methylene Blue (MB) and Toluidine Blue (TB) fluoresced at 638nm excitation wavelength. The results indicate that simple clinical chemicals can be used to enhance the ability of confocal fluorescence microscopy to differentiate nuclear morphology in living cells (Figure 1). Figure 1A shows comparative confocal images of normal (NHBE) and cancer cells (HaCaT, SCC-15, HeLa) stained either with AH or CV. AH showed a clear nuclear staining with a difference in the nuclear morphology in which normal cells (NHBE) had uniform round nuclei whereas cancer cells had nuclei of a different size and shape (nuclear pleomorphism) and a marked nucleolar staining (nucleolar prominence). The cytoplasm is faintly visible as a noticeable background allowing reasonable nuclear-to-cytoplasm contrast. CV showed cytoplasmic uptake only in normal and cancer cells, leaving a void in the center. Using H2B-GFP transfected HeLa cells specifically with intranuclear GFP expression, we confirmed exclusive cytoplasmic staining of CV in living cells (Figure 1B). Thus, CV

allows negative visualization of nuclei morphology. MB and TB staining mainly resulted in near infra-red fluorescence in the cytoplasmic compartment (Figure 1C). However, their fluorescence yield was low. Topical application of FS resulted in diffusive staining of both the cytoplasm and the nucleus, which made it difficult to outline its nuclear morphology and other details (Figure 1C).

Only AH and CV were then selected for the evaluation of human oral ex vivo samples (Figure 2). With AH staining, individual cell nuclei were easily visible as bright dots in fluorescence images obtained with confocal microscopy (Figures 2A and 2B). On one hand, the AH stained-transversal section of the oral mucosa showed multi-layering and uniform polarity of the differentiated cells that distinguished the squamous epithelium (Figure 2C). On the other hand, the uptake of CV by the epithelial cells of the human oral mucosa was low (Figures 2D and 2E) with poor nuclear-to-cytoplasm contrast (Figure 2E). As shown in Figure 2F, occasional cells displayed bright cytoplasmic fluorescence in CV staining, but their morphology suggested that they were Langerhans cells and not epithelial cells. Finally, we selected AH as the best contrast agent to be used in ex vivo confocal imaging.

### **Confocal imaging histology of normal oral mucosa using Acriflavine Hydrochloride**

The lining epithelium of the oral cavity is stratified squamous epithelium which consists of flattened (squamous) cells on the surface overlying multiple layers of cells that are usually cuboidal toward the base of the epithelium. Using confocal microscopy after topical application of AH on both the surface and basal sides of the ex vivo specimen and allowing a longer time of incubation for better dye penetration, we successfully visualized all representative layers of the squamous epithelium from an eagle's eye point of view. The cells on the basal layer were crowded with small, monotonous and spherical nuclei (Figure 3A). The basal cells continuously produced new differentiated cells with nuclei that appeared spherical and larger in size a wider inter-nuclear space (Figure 3B). As these cells were pushed upwards into overlying layers, they became flatter and contained elliptical nuclei with an even wider inter-nuclear space and a more prominent cell-cell border with a typical squamous shape (Figure 3C). A good analogy for their shape is paving stones (squamous epithelium has also been called "pavement" epithelium). When the cells reached the top, their nuclei were either pyknotic, small and dense (Figure 3D) or absent (Figure 3E). These are dead cells that have been sloughed off and replaced by cells from below. The connective tissue underlying the squamous epithelium was composed of spindle-shaped cells with elongated nuclei (Figure 3F). Similar layering and stratification can also be observed in Figure 2C.

### **Histopathology-like confocal imaging of oral dysplasia**

Thirty-three lesional and normal human oral mucosa specimens were obtained from thirteen patients during excisional surgery. Although superficial topical application of AH strongly stained the epithelial cell nuclei, the dye did not penetrate deeply into the stratified epithelium, thereby limiting the imaging depth to the top 50–100  $\mu\text{m}$ . We recorded the confocal microscopy images at a standard depth of 50  $\mu\text{m}$  for each specimen. Figure 4 shows representative sets of confocal images with the corresponding histology using formalin-fixed, paraffin-embedded H&E staining at a definitive pathology diagnostic level from normal, moderate dysplasia to severe dysplasia. In confocal imaging at 50  $\mu\text{m}$  from the surface, the normal epithelium was characterized by regularly spaced cell nuclei with uniform size and shape (Figure 4B); moderate dysplasia was characterized by an increase in the density of irregularly-spaced nuclei with an occasional irregular nuclear border (Figure 4D); and severe dysplasia was characterized by its intense nuclear fluorescent staining (hyperchromasia), variable nuclear shape and size (pleomorphism), and an increased density of irregularly-spaced nuclei (Figure 4F). Table 1 correlates the description of the nuclear

morphological finding in confocal imaging with the final pathology in H&E histology for all the cases. The confocal microscopy was able to detect severe dysplasia lesions with 100% accuracy. Normal mucosa, hyperplasia and mild dysplasia appeared identical at the confocal examination of the surface epithelium. The confocal descriptions in moderate dysplasia were inconsistent.

### Quantitative histological analysis

To better quantify the changes observed above, we have also used the Getafics image analyzer software to objectively calculate the cellular density (Figure 5A). There was an increase in the median of cellular density with the severity of dysplasia:  $5.1 \times 10^{-4}$ ,  $4.7 \times 10^{-4}$ ,  $5.1 \times 10^{-4}$ ,  $13.3 \times 10^{-4}$ , and  $28.1 \times 10^{-4}$  nuclei per square mm in normal, hyperplasia, mild dysplasia, moderate dysplasia, and severe dysplasia respectively (Figure 5B). There is a significant difference of the cellular density in the high-grade dysplasia group compared to the low-grade dysplasia group and normal/hyperplasia group ( $P = 0.0001$ ) (Figure 5C). There is no statistically significant difference in the cellular density between the low-grade lesions (mild and moderate dysplasia). Figure 5D shows the scattergram of cellular density in the 3 main groups of progression risk and demonstrates the ability of the cellular density to clearly discriminate the high-grade dysplasia group among the others (Figure 5D). These findings are consistent with our observation and give a more objective approach to observe the change among various histological degrees.

## DISCUSSION

Central principles in the cancer management are the early detection of pre-malignant disease and complete or maximal extirpation of diseased tissue. Optical imaging technologies have potential applications that would substantially improve current medical practice and optimize cancer management, particularly for early detection and screening.

Techniques such as reflectance spectroscopy<sup>15</sup>, fluorescence spectroscopy<sup>16</sup> and autofluorescence<sup>17</sup> are being used to extract information from oral mucosa on the basis of the interaction of light with endogenous tissue fluorophores. However, *in vivo* confocal microscopy reveals the actual cellular structures and as such is a form of *in vivo* histology. This implies the application of exogenous fluorophores that stain cellular structures in order to provide strong and clear cellular contrast that is sufficient to allow real-time interaction with live imaging streams.

Targeted, optically active molecular probes are currently being developed to specifically label extra- and intracellular biomarkers of cancers<sup>18</sup>. This new emerging technique will enable to acquire fluorescent optical images of specific molecular targets while still providing morphologic context of the tissue. In the meantime, a limited number of fluorescent dyes are registered for clinical use in real time confocal microscopy. In the present study, we showed that Acriflavine Hydrochloride provides the best cellular contrast by preferentially staining the nuclei of the epithelium. Acriflavine has a long history of clinical use as an antiseptic agent<sup>19</sup>, a comprehensive safety data record and is being used widely for confocal endomicroscopy in gastro-intestinal tract<sup>20</sup>.

To be effective in the use of this technology, the future physician will need to be familiar with detailed histological appearances of normal human oral mucosa. This, in turn, will lead to a new breed of “clinician pathologist” capable of defining tissue changes accompanying dysplasia on real-time optical imaging. Because confocal microscopy offers images of living samples by reducing out-of-focus light from above and below the focal plane, we were able to generate optical slices and provide a multilayered atlas of oral epithelium images consisting of *en face* histology-like sections as per standard histology slides. We have

demonstrated that this technology is reliable to define morphological characteristics of each cellular layer of the human oral mucosa, from the surface to the basal layer.

The stratified squamous epithelium of the oral mucosa, with its multiple layers of cells, is a diffusive cell barrier allowing fluids to pass through gradually. Subsequently, limitations of the topical application of fluorophores stain in a short length of time can include limited infiltration depth. In our study, topical application has allowed the observation of surface epithelium structures from 50 to 100  $\mu\text{m}$  deep. For normal anatomy appreciation, we managed to stain the basal layer by applying the dye on the bottom side of the *ex vivo* specimens but this is not reproducible *in vivo*. Imaging depth could be increased by intravenous administration of the fluorophore dye, as it is being done with Fluorescein Sodium for gastro-intestinal endomicroscopy<sup>20</sup>. However, AH does not have the approval for intravenous delivery and the preparation of a preliminary IV line would not be convenient for massive screening strategy in the clinical settings. Most importantly, our results showed that even limited depth imaging of the surface epithelium displays sufficient diagnostic informations to detect high-grade dysplasia.

With confocal microscopy, malignant nuclei were clearly identifiable as they showcased increased fluorescence intensity and polymorphism in size and shape. These confocal morphometric features are consistent with classical descriptions of malignant nuclei in standard H&E examination. Severe dysplasia lesions were easily distinguished because dysplastic cells reach the top of oral epithelium and their identification was then possible by the superficial staining. However, it was challenging to make a clear distinguishing of mild and moderate dysplasia based on nuclear features at 50  $\mu\text{m}$  from the surface. This is because the fact that the stain did not constantly penetrate into deeper layer of oral epithelium. Moderate dysplasia is considered to be a slightly elevated risk of progression comparing to mild dysplasia. We had to consider additional parameters in order to improve the accuracy of moderate dysplasia detection.

The application of this work to clinical practice is limited by the *ex vivo* tissue model and the likely image quality of an *in vivo* device. Images of freshly excised *ex vivo* tissue samples are likely to be different from those imaged *in vivo*. There may be differences in tissue morphology and dye uptake post resection, however, our experience has shown these differences are small. The image quality (field-of-view and confocality) of a small handheld confocal wand suitable for clinical deployment will likely be inferior compared to those images presented here using bench-top confocal microscope. Due to space constrains in the oral cavity, it is technically challenging to construct a handheld wand with the same optical performance as a microscope objective. Initial results from our handheld device suggest image quality is degraded only slightly (due to decrease in confocality) compared to bench-top microscopy and that the spatial arrangement of cells is still clear.

We have started testing a handheld confocal wand for *in vivo* imaging of potentially malignant lesions. Initial results suggest that *in vivo* confocal microscopy may have the potential to significantly improve biopsy site selection, particularly in the cases of potentially malignant lesions where determination of the worst (or most at risk) area to biopsy can be problematic, leading to improved diagnosis by histopathology. In addition, the technology could offer real-time determination of surgical margins and the ability to monitor recurrence or progression, and response to therapy, in real time. Moreover, the handheld confocal wand could also be used *in vivo* to image molecular targets correlated with carcinogenesis.

Quantitative pathology is a computer-driven approach that uses image analyzer software to objectively assess both of the cytological and architectural features of histological sections

of oral mucosa<sup>21</sup>. Because the interpretation of confocal images would be dependent on the observer's experience, the accuracy of diagnostic would be subject to a learning curve similar to that for histopathology. We propose the use of image analyzers as an adjunct tool to assist the users of real time confocal microscopy. The quantitative measurement of cellular density alone would be able to correlate the superficial confocal microscopy appearance with the presence of high-grade dysplasia. Thus, the combination of nuclear morphologic features with nuclear density would optimize the diagnostic performance of confocal microscopy.

In conclusion, confocal microscopy of the human oral mucosa using AH as the contrast agent can provides real-time imaging of oral mucosa architecture and nuclear morphology. This technology can help detect precancerous lesions that are at risk of cancer progression. Pending further clinical investigation and technological improvement, real-time confocal microscopy may become a useful adjunct to detect occult oral dysplasia, direct biopsy, delineate excision margins and surveillance. As with all new technologies, *in vivo* confocal microscopy requires careful testing and thorough evaluation before clinical incorporation in the workplace. A clinical trial using a hand-held confocal probe is being implemented in our institute to evaluate the impact of this promising technology in the clinical practice.

## Acknowledgments

This work was supported by the Canadian Institutes of Health Research and grant number P01-CA-82710-09 from the National Cancer Institute. The HaCaT cell line was generously provided by Prof. Dr. Norbert Fusenig, German Cancer Research Center (Heidelberg, Germany).

## Abbreviations

<b>AH</b>	Acridine Hydrochloride
<b>CV</b>	Cresyl Violet
<b>TB</b>	Toluidine Blue
<b>MB</b>	Methylene Blue
<b>FS</b>	Fluorescein Sodium
<b>H&amp;E</b>	Hematoxylin and eosin stain

## References

1. Ferlay, J.; Shin, H.; Bray, F.; Forman, D.; Mathers, C.; Parkin, D. GLOBOCAN 2008 v2.0, Cancer Incidence and Mortality Worldwide. IARC CancerBase No 10. 2010. [Internet] ed. Available: <http://globocan.iarc.fr>
2. American Cancer Society. Cancer facts and figures 2012. American Cancer Society; Atlanta, GA: 2012. Publication No. 5008.07
3. Day GL, Blot WJ. Second Primary Tumors in Patients with Oral-Cancer. *Cancer*. 1992; 70:14–19. [PubMed: 1606536]
4. Wright JM. A review and update of oral precancerous lesions. *Tex Dent J*. 1998; 115:15–19. [PubMed: 9667207]
5. Zhang L, Poh CF, Williams M, Laronde DM, Berean K, Gardner PJ, et al. Loss of heterozygosity (LOH) profiles: validated risk predictors for progression to oral cancer. *Cancer Prev Res (Phila)*. 2012; 5(9):1081–1089. [PubMed: 22911111]
6. Guillaud M, Zhang L, Poh C, Rosin MP, Macaulay C. Potential use of quantitative tissue phenotype to predict malignant risk for oral premalignant lesions. *Cancer Research*. 2008; 68(9):3099–3107. [PubMed: 18451134]

7. Schepman KP, Van der Meij EH, Smeele LE, Van der Waal I. Malignant transformation of oral leukoplakia: a follow-up study of a hospital-based population of 166 patients with oral leukoplakia from The Netherlands. *Oral Oncology*. 1998; 34:270–275. [PubMed: 9813722]
8. Hurlstone DP, Tiffin N, Brown SR, Baraza W, Thomson M, Cross SS. In vivo confocal laser scanning chromo-endomicroscopy of colorectal neoplasia: changing the technological paradigm. *Histopathology*. 2008; 52(4):417–426. [PubMed: 17903203]
9. Tan J, Delaney P, McLaren WJ. Confocal endomicroscopy: a novel imaging technique for in vivo histology of cervical intraepithelial neoplasia. *Expert Rev Med Devices*. 2007; 4(6):863–871. [PubMed: 18035951]
10. Gerger A, Hofmann-Wellenhof R, Samonigg H, Smolle J. In vivo confocal laser scanning microscopy in the diagnosis of melanocytic skin tumours. *Br J Dermatol*. 2009; 160(3):475–481. [PubMed: 19183178]
11. Inoue H, Kudo S, Shiokawa A. Technology insight: laser scanning confocal microscopy and endocytoscopy for cellular observation of the gastrointestinal tract. *Nat Clin Pract Gastroenterol Hepatol*. 2005; 2:31–36. [PubMed: 16265098]
12. Chen C, Okayama H. High-efficiency transformation of mammalian cells by plasmid DNA. *Mol Cell Biol*. 1987; 7:2745–2752. [PubMed: 3670292]
13. Poh CF, Durham JS, Brasher PM, Anderson DW, Berean LW, MacAulay CE, et al. Canadian optically-guided approach for oral lesions surgical (COOLS) trial: study protocol for a randomized controlled trial. *BMC Cancer*. 2011; 11:462. [PubMed: 22026481]
14. Kamalova R, Guillaud M, Haskins D, Harrison A, Kemp R, Chiu D, et al. A Java application for tissue section image analysis. *Computer Methods and Programs in Biomedicine*. 2005; 77:99–113. [PubMed: 15652632]
15. Jayanthi JL, Nisha GU, Manju S, Philip EK, Jeemon P, Baiju KV, et al. Diffuse reflectance spectroscopy: diagnostic accuracy of a non-invasive screening technique for early detection of malignant changes in the oral cavity. *BMJ Open*. 2011; 1(1):e000071.
16. Lane P, Follen M, Macaulay C. Has fluorescence spectroscopy come of age? A case series of oral precancers and cancers using white light, fluorescent light at 405nm, and reflected light at 454nm using the Trimira Identafi 3000. *Gen Med*. 2012; 1:S25–S35.
17. Poh CF, Ng SP, Williams PM, Zhang L, Lalonde DM, Lane P, et al. Direct autofluorescence visualization of clinically occult high-risk oral premalignant disease using a simple hand-held device. *Head Neck*. 2007; 29(1):71–76. [PubMed: 16983693]
18. Hellebust A, Richards-Kortum R. Advances in molecular imaging: targeted optical contrast agents for cancer diagnostics. *Nanomedicine (Lond)*. 2012; 7(3):429–445. [PubMed: 22385200]
19. Kawai M, Yamagishi J. Mechanisms of action of Acriflavine: electron microscopy study of cell wall changes induced in *Staphylococcus aureus* by Acriflavine. *Microbiol Immunol*. 2009; 53(9): 481–486. [PubMed: 19703241]
20. Gheonea DI, Saftoiu A, Ciurea T, Popescu C, Georgescu CV, Malos A. Confocal laser endomicroscopy of the colon. *J Gastrointest Liver Dis*. 2010; 19(2):207–11. [PubMed: 20593059]
21. Guillaud M, Zhang L, Poh C, Rosin MP, Macaulay C. Potential use of quantitative tissue phenotype to predict malignant risk for oral premalignant lesions. *Cancer Research*. 2008; 68(9): 3099–3107. [PubMed: 18451134]

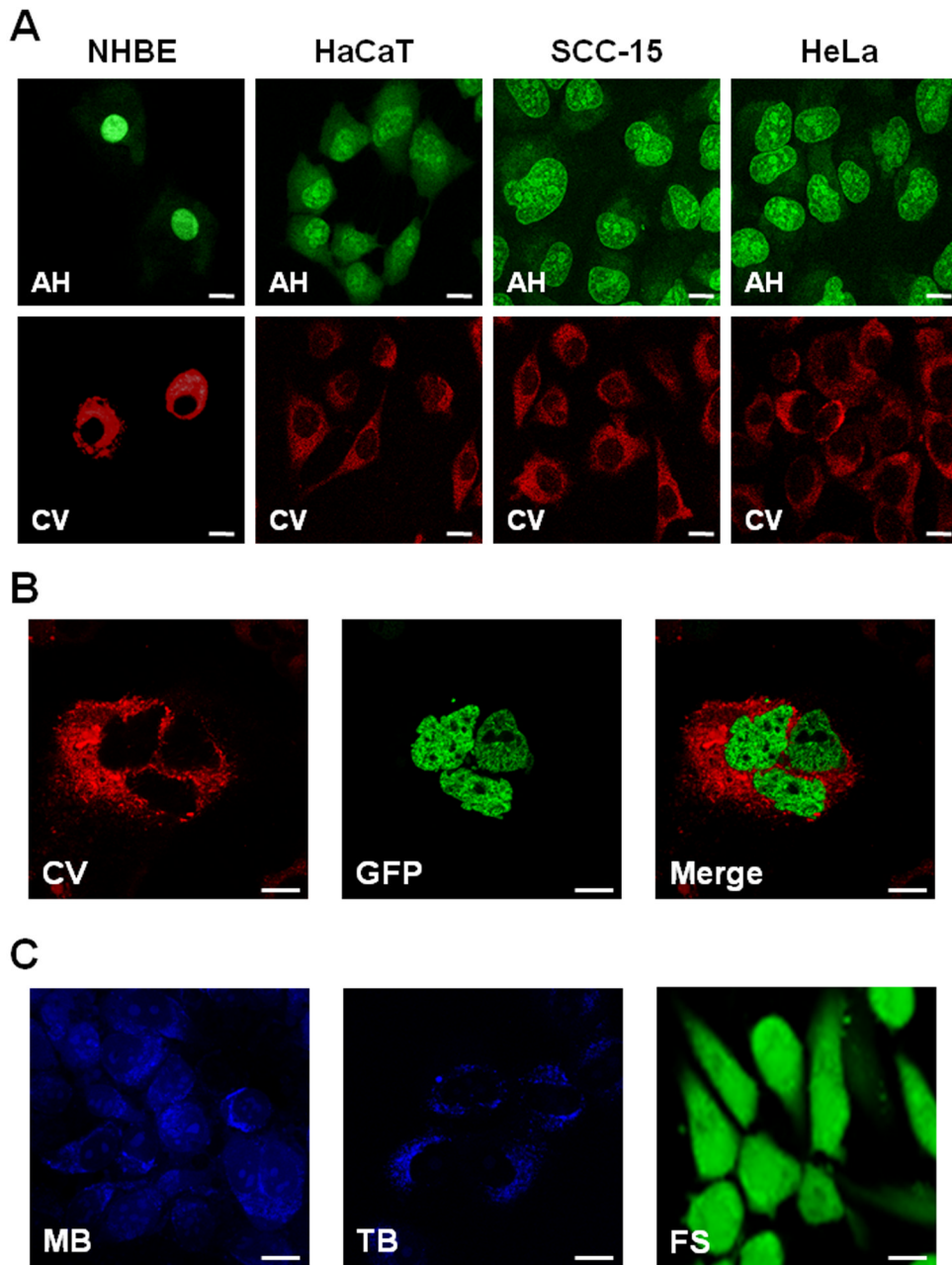


**Figure 1. In vitro contrast agent testing**

(A) Comparative confocal images of cultured normal (NHBE) and cancer cells (HaCaT, SCC-15, HeLa) from left to right, typically stained with Acriflavine Hydrochloride (AH; upper panel) or Cresyl Violet (CV; lower panel). (B) Cultured H2B-GFP expressing cells stained with CV: left, CV (red fluorescence) only; middle, GFP (green fluorescence); right, co-localization of CV and GFP. (C) Cultured cells typically stained with Methylene Blue (MB; left), Toluidine Blue (TB; middle) and Fluorescein Sodium (FS, right). The common scale bar is 20  $\mu$ m wide.

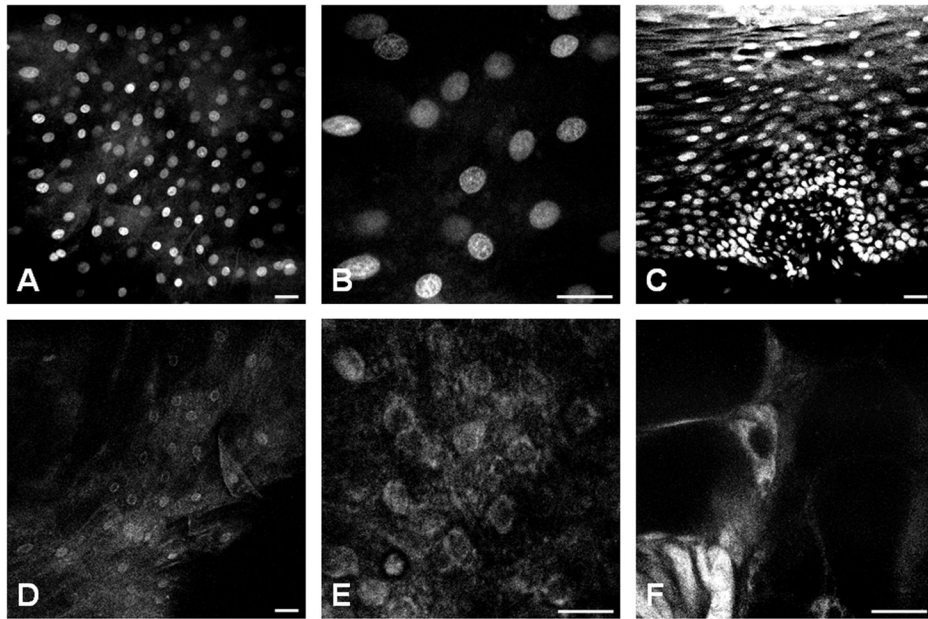


**Figure 2. Ex vivo contrast agent testing**

Confocal imaging comparing the nuclear morphology of the oral epithelium after topical application of Acriflavine Hydrochloride (A–C) or Cresyl Violet (D–F). A & B, an *en face* image taken from a normal epithelium at 50  $\mu\text{m}$  from the surface and B is from the same field of view with magnified A. C, an on edge transversal section of oral mucosa showed multilayering and uniform polarity of differentiated cells that distinguish the stratified squamous epithelium from the basal cell layer (closely packed low cuboidal nuclei at the bottom), the spinous cell layer (evenly spaced out, slightly ovoid shaped nuclei with their long axis parallel to the surface), and the parakeratinized superficial layer (tightly packed with smaller, elongated nuclei at the top). D & E, an *en face* image taken from a normal epithelium at 50  $\mu\text{m}$  from the surface show fainter cytoplasmic and perinuclear uptake of CV (E is the same field of view with magnified D). F, a star-like cell with elongated cytoplasmic protrusion shows bright intra-cytoplasmic fluorescence. This cell, according to its morphology and intraepithelial location, is consistent with a Langerhans (or antigen presenting) cell. The common scale bar is 50  $\mu\text{m}$  wide.

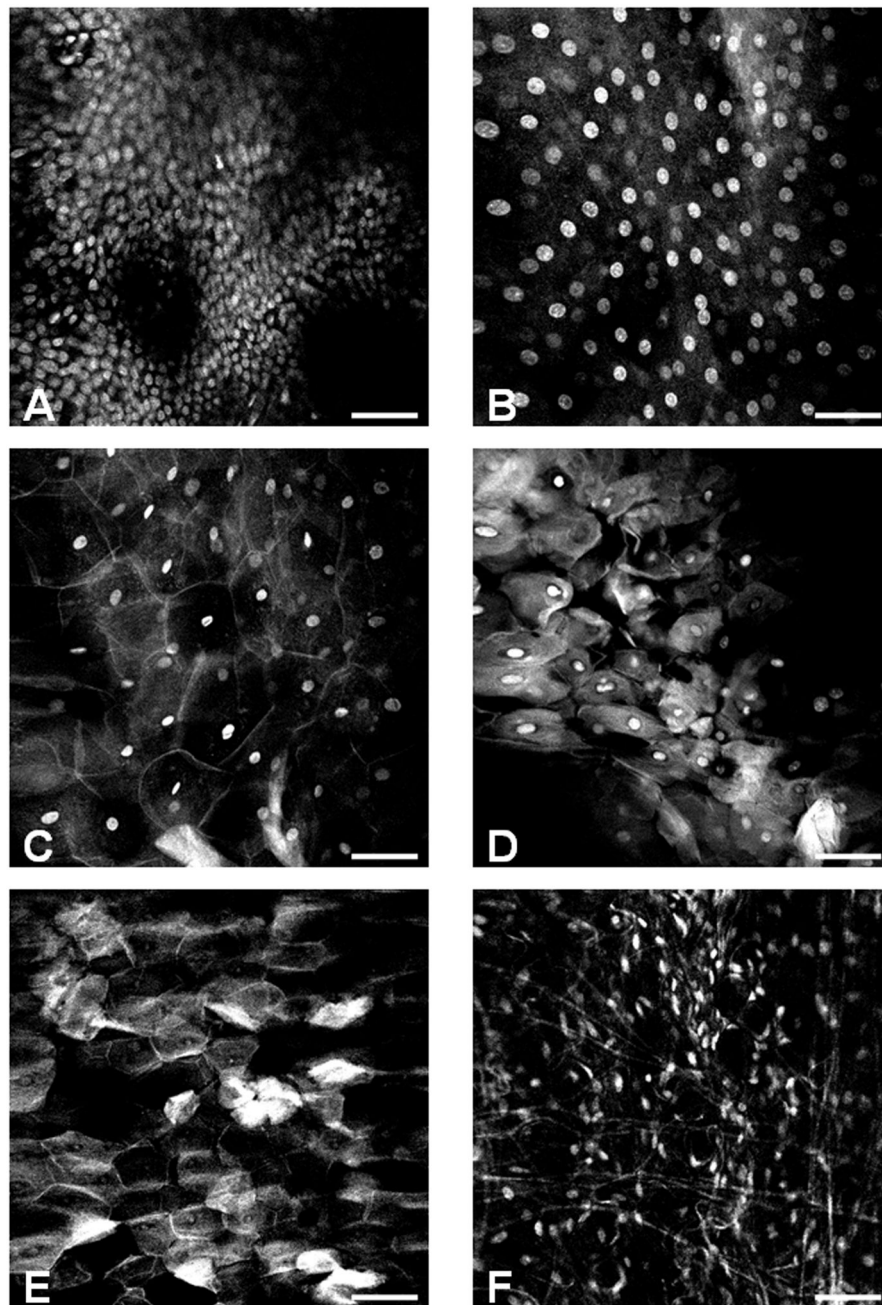


**Figure 3. Representative confocal imaging histology of normal oral mucosa**

An atlas of the oral mucosa displaying different layers of the stratified squamous epithelium and subepithelial connective tissue: (A) basal cell layer, (B) parabasal cell layer (50  $\mu\text{m}$  above A), (C) spinous cell layer, (D–E) superficial parakeratinized or keratinized layer, (F) Subepithelial connective tissue. The scale bar is 100  $\mu\text{m}$  wide.

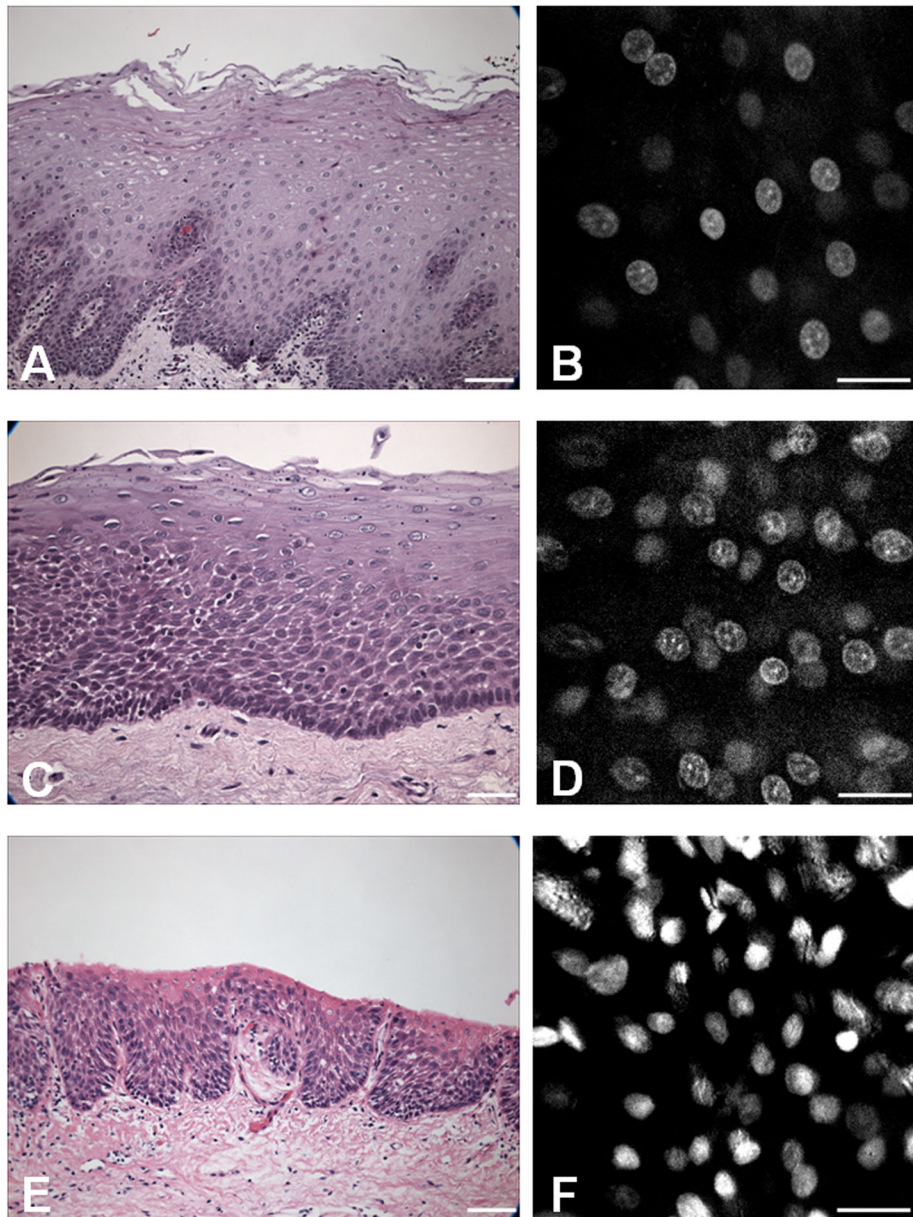


**Figure 4. Histopathology-like confocal diagnosis of oral dysplasia**

Features of the oral epithelium confocal imaging are correlated with conventional histology (H&E staining) for normal mucosa (A–B), moderate dysplasia (C–D), and severe dysplasia (E–F). The scale bar is 100  $\mu\text{m}$  wide for H&E images and 50  $\mu\text{m}$  wide for confocal images.

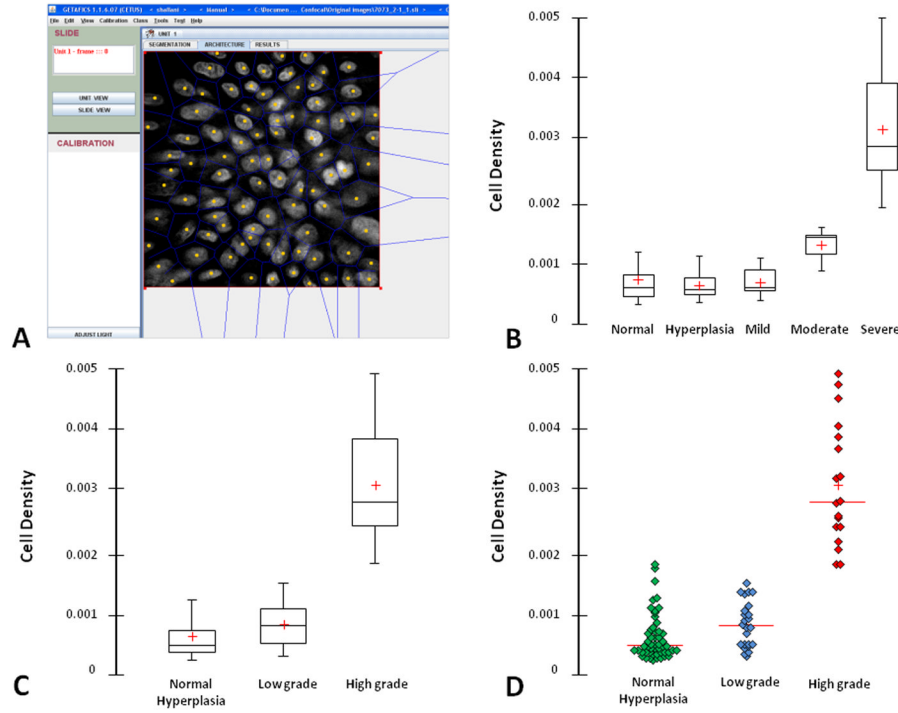


**Figure 5. Quantitative histological analysis**

(A) Interface of the Getafics Imaging Software showing the resulting segmentation on Voronoi diagram from a confocal microscopy-acquired image. The yellow dots are the centre of the gravity of each nucleus and the blue lines are for the calculated cell boundaries, called Voronoi. At the region of interest of each confocal image, the program can automatically calculate the cellular density (number of nucleus per square mm). (B) Box plot of cellular density of varying histology from no dysplasia, hyperplasia, mild dysplasia, moderate dysplasia, and severe dysplasia. Error bar, 5<sup>th</sup> and 95<sup>th</sup> percentiles; box, central cross, 50<sup>th</sup> percentile and median level; red cross, mean. (C) Box plot of cellular density of the 3 main groups of progression risk varying from normal/hyperplasia; low-grade dysplasia (mild and moderate dysplasia) and high-grade dysplasia (severe dysplasia). Error bar, 5<sup>th</sup> and 95<sup>th</sup> percentiles; box, central cross, 50<sup>th</sup> percentile and median level; red cross, mean. (D) Scattergram of high-grade dysplasia against low-grade dysplasia and normal/hyperplasia using cellular density as discriminant factor.

Table 1

Clinical, confocal and histological characterization of the study cases.

Cases	Age (years)	Sex	Smoking History	Smoking Details	Current Heavy Drink <sup>a</sup>	Site	Samples	Nuclear features in confocal imaging			H&E histology
								Density	Cell-Cell spacing	Size and shape	
Patient 1	82	M	FS	48 Pack-year, quit for 10 years	N	Tongue	# 1	markedly increased	irregular	variable	Severe dysplasia
Patient 2	50	M	FS	31 Pack-year, quit for 1 year	N	Floor of Mouth	# 1	normal	regular	uniform	Normal mucosa
Patient 3	68	M	S	67 Pack-year	N	Floor of Mouth	# 1	markedly increased	irregular	variable	Severe dysplasia
							# 2	slightly increased	irregular	uniform	Moderate dysplasia
							# 3	normal	regular	uniform	Hyperplasia
							# 4	normal	regular	uniform	Hyperplasia
							# 5	slightly increased	irregular	uniform	Moderate dysplasia
							# 6	markedly increased	irregular	variable	Severe dysplasia
Patient 4	61	M	FS	25 Pack-year, quit for 13 years	N	Soft Palate	# 1	normal	regular	uniform	Mild dysplasia
							# 2	normal	regular	uniform	Hyperplasia
							# 3	normal	regular	uniform	Hyperplasia
Patient 5	42	F	NS	-	N	Tongue	# 1	normal	regular	uniform	Normal mucosa
							# 2	normal	regular	uniform	Normal mucosa
							# 3	normal	regular	uniform	Normal mucosa
							# 4	normal	regular	uniform	Normal mucosa
Patient 6	70	M	FS	50 Pack-year, quit for 1 year	N	Soft Palate	# 1	normal	regular	uniform	Mild dysplasia
							# 2	normal	regular	uniform	Moderate dysplasia
Patient 7	34	F	NS	-	N	Tongue	# 1	normal	regular	uniform	Normal mucosa
							# 2	normal	regular	uniform	Normal mucosa
Patient 8	83	F	NS	-	N	Tongue	# 1	normal	regular	uniform	Mild dysplasia
							# 2	normal	regular	uniform	Mild dysplasia
Patient 9	68	F	FS	30 Pack-year, quit for 28 yrs	N	Tongue	# 1	markedly increased	irregular	variable	Severe dysplasia

Cases	Age (years)	Sex	Smoking History	Smoking Details	Current Heavy Drink <sup>a</sup>	Site	Samples	Nuclear features in confocal imaging			H&E histology
								Density	Cell-Cell spacing	Size and shape	
Patient 10	64	M	S	46 Pack-year	Y	Soft Palate	# 2	markedly increased	irregular	variable	Severe dysplasia
Patient 11	49	M	NS	-	N	Tongue	# 1	normal	regular	uniform	Mild dysplasia
							# 2	markedly increased	irregular	variable	Severe dysplasia
Patient 12	70	M	FS	33 Pack-year, quit for 18 years	N	Tongue	# 1	normal	regular	uniform	Normal mucosa
							# 2	normal	regular	uniform	Normal mucosa
Patient 13	84	M	FS	43 Pack-year, quit for 24 years	N	Tongue	# 1	markedly increased	irregular	variable	Severe dysplasia
							# 2	markedly increased	irregular	variable	Severe dysplasia

<sup>a</sup> Current heavy drinker: 3 units/day; 1 unit = 1 glass of wine, 1 can of beer, or 1 shot of liquor